Department of Physics and Astronomy
University of Heidelberg

Bachelor Thesis in Physics
submitted by

Michael Schork

born in Mosbach, Baden (Germany)

2014

Hints for collective effects in identified particle spectra from p–Pb collisions at 5.02 TeV

Abstract

First hints for collective dynamics in high-multiplicity p-Pb collisions at LHC were observed in two-particle correlations of unidentified particles. We present a systematic study of Blastwave-fits to identified particle spectra from p-Pb and Pb-Pb collisions as measured by ALICE at the LHC. While in Pb-Pb collisions, a large number of particles can be commonly described by a single set of parameters including mass A=2 and A=3 nuclei, also spectra from high-multiplicity p-Pb collisions allow for a description within this rather simple model. Finally, we give predictions for spectra and the nuclear modification factor of mesons carrying a charm or bottom quark.

Kurzfassung

Erste Hinweise auf kollektive Dynamik in p-Pb Kollisionen mit hoher Multiplizität am LHC wurden zuerst in zwei-Teilchen Korrelationen von Spuren nicht identifizierter Teilchen beobachtet. Wir stellen eine sytematische Studie von Blastwave Fits an Spektren identifizierter Teilchen von p-Pb und Pb-Pb Kollisionen, wie sie von ALICE am LHC gemessen wurden, an. Wärend in Pb-Pb Kollisionen eine große Anzahl von Teilchen, inklusive Kerne mit Massenzahl A=2 und A=3, durch einen gemeinsamen Satz von Parametern beschrieben werden können, sind auch die Spektren von p-Pb Kollisionen hoher Multiplizität durch dieses recht einfache Model beschreibbar. Schließlich stellen wir Vorhersagen für die Spektren und den nuklearen Modifikationsfaktor von Mesonen mit Charm- und Bottom-Quarks bereit.

This Bachelor Thesis has been carried out by Michael Schork at the
Physikalisches Institut of the University of Heidelberg
under the supervision of
Dr. Kai Schweda

Contents

1 Introduction

In everyday life we typically think of three common states of matter: solids, liquids and gases. We can easily transform matter between these states by changing external conditions such as temperature and pressure, since phase transitions between the different states occur at specific conditions. The melting of ice to liquid water and the vaporization at the boiling point with rising temperature are simple examples. When increasing the enthalpy of the system even further, the gas will transform again forming a plasma, in which the electrons are freed from their respective nuclei and free to move around. This state of matter seems not to be as common in nature, but is in fact observable day by day in fire, lightnings, or even used in plasma televisions.

Except for these common states of matter, there is a variety of other states possible at extreme conditions. At temperatures not far above absolute zero, Bose-Einstein condensates can be observed, while at extremely high temperatures and densities quarks and gluons, that are usually confined into hadrons, become free, forming another state of matter called quark-gluon plasma (QGP). The conditions needed to observe this plasma, where not the electromagnetic force between electrons and nuclei, but the strong interaction of quarks and gluons is overcome, may be reached in high energetic heavy-ion collisions at the Relativistic Heavy Ion Collider (RHIC) and the Large Hadron Collider (LHC). When colliding protons, the system size is too small to create a QGP. Thus the only way of creating it in the laboratory is colliding heavy nuclei such as lead in case of the LHC.

The p-Pb collisions, measured in a run at LHC in the beginning of 2013, provide an intermediate system in terms of size and density. It can be compared to either pp and Pb–Pb, while it is not clear, if a QGP is formed in such collisions.

After its formation, the QGP will only last for a few fm/c while rapidly cooling and expanding. It is therefore not directly observable, but information on the medium properties are accessible by tracing the particles originating from it, when temperature and density are low enough again.

In this thesis, the particle spectra measured by ALICE will be described in terms of their collective medium properties by a Blastwave-Model [1] in Pb-Pb as well as p-Pb.

We will investigate if hints for collective effects recently found in angular correlations [2, 3] in the latter can be confirmed by inspecting spectra within this simple model.

This thesis is organized as follows: After shortly introducing the Blastwave-Model in section 2, we will describe the experimental data used in the analysis in section 3. The results will be presented in section 4, starting with the analysis of multiplicity dependent Pb–Pb spectra and an analysis of 17 particles in central Pb–Pb events, followed by a comparison to what is found in p-Pb multiplicity dependent spectra and predictions based on this analysis. Finally, section 5 will give a summary.

2 Blastwave-Model

A relativistic measure for the number of particles produced in a collision is the invariant yield $E\frac{d^3N}{d^3\vec{p}}$ which is equivalent to $\frac{1}{2\pi p_T}\frac{d^2N}{dp_T dy}$ as well as $\frac{1}{2\pi m_T}\frac{d^2N}{dm_T dy}$ in an azimuthally symmetric situation, where p_T is the transverse momentum and $m_T = \sqrt{m^2 + p_T^2}$ the transverse mass. Natural units are used, so $\hbar = c = k_B = 1$.

To describe the transverse momentum distributions of the analyzed particle spectra we will use the Blastwave-Model as described in [1]. We want to address particles produced at mid-rapidity and assume a thermal particle source, which is boost-invariant along the beam direction.

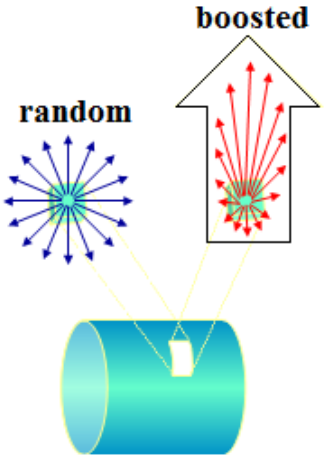

Figure 2.1: Cylindrical source; each volume element thermally emits particles isotropically and is boosted in transverse direction at the same time.

In the plane transverse to the beam, we assume a radial velocity profile

$$\beta(r) = \beta_s(\frac{r}{R})^n$$

with the maximum surface velocity β_s, the radial extension R of the fireball and a free parameter n describing the shape of the velocity profile, such that $n = 1$ means a linearly increasing velocity. The influence of n on the shape of the profile is shown in Figure 2.2. It evolves from a rather flat function for $n = 0.2$ over a root-shaped curve for $n = 0.5$ and a linear increase at $n = 1$ to a parabola at $n = 3$, such that the inside of the source is no longer taking part in the rapid expansion on the outside.

We can now define a boost angle $\rho = tanh^{-1}\beta$ which - together with a boost in longitudinal direction by η - results in a velocity field

$$u^{\nu}(\rho,\eta) = (\cosh\rho\ \cosh\eta,\ \vec{e_r}\sinh\rho,\ \cosh\rho\ \sinh\eta)\,,$$

where $\vec{e_r}$ is a two-dimensional unit vector in the transverse plane.

The thermal part of the source, emitting particles in all directions as shown in Figure 2.1, is assumed to follow a Boltzmann-Distribution and is thus described by a term proportional to $e^{-(E/T)}$, boosted by the velocity field, such that the invariant yield is an integral over all emission points of the source

$$\frac{1}{2\pi p_T}\frac{d^2N}{dp_T dy}\ \propto\ \int_{\sigma} e^{-(u^{\nu}p_{\nu})/T}\ p^{\lambda}\ \mathrm{d}\sigma_{\lambda}\,,$$

where σ is a hypersurface separating the inner reaction phase from the free streaming particles on the outside. The final normalization constant making both sides equal does not affect the shape of the distribution with the physical model parameters we are interested in and will therefore be another free parameter in the model. Since a larger source will only emit a larger number of particles with the same shape in transverse momentum, the source radius R is also arbitrary. In this simple approach, an instantaneous freeze-out is assumed and σ can be parametrized in cylindrical coordinates $0 \le r \le R,\ 0 \le \phi < 2\pi$ and $-Z \le \zeta \le Z$ as

$$\sigma^{\nu}(r,\phi,\zeta)\ =\ (\ t(\zeta),\ r\ \cos\phi,\ r\ \sin\phi,\ z(\zeta)\ )\,,$$

while the dependence on ζ allows for a more general shape in longitudinal direction. The azimuthal symmetry of the system can be used to integrate over azimuth ϕ first, which results in a modified Bessel function of the first kind I_0, while the integration over the parameter ζ results in one of the second kind and first order K_1. The integration over the radial extension can only be done numerically and the final analytical expression is

$$\frac{1}{2\pi p_T}\frac{d^2N}{dp_T dy}\ \propto\ \int_0^R\ r\ \mathrm{d}r\ m_T\ I_0\left(\frac{p_T\ \sinh\rho}{T}\right)\ K_1\left(\frac{m_T\ \cosh\rho}{T}\right)\,.$$

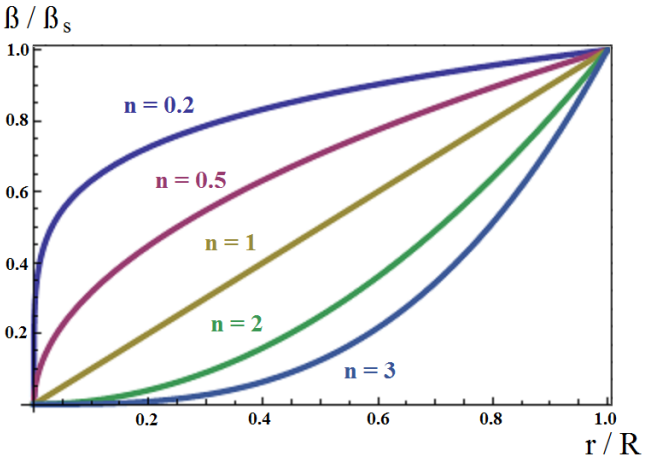

Figure 2.2: Radial velocity profile; shown for different shape parameters n.

The numerical integration is carried out by arbitrarily setting the source radius to $R = 10\,\text{fm}$ and evaluating it at 100 points with constant spacing $dr = 0.1\,\text{fm}$. At each point the integrand is computed and added up.

We will now try to describe the experimental spectra of multiple particles with this Blastwave-Model. Information on the collective properties of the medium the particles originate from is derived from the following fit parameters: The kinetic freeze-out temperature-parameter T, the surface velocity of the expanding system β_s and the shape parameter of the velocity profile n. Since the normalization parameter, describing the total yield, is not universal for different particles it will be adjusted individually.

Typical values for the temperature at LHC energies are about 0.1 GeV which corresponds to $1.2 \cdot 10^{12}\,\text{K}$ while the surface velocity turns out to be up to 88% the speed of light in our fits. In this analysis, the average transverse flow velocity $\langle\beta_T\rangle$ will be used most of the time, which gives a better description of the medium properties and is related to the surface velocity β_s by

$$\langle\beta_T\rangle \;=\; \frac{2\beta_s}{n+2}\,,$$

with the associated shape parameter n.

3 Experimental Data

The data for the following analysis comes mainly from two publications. First there are the multiplicity dependent transverse momentum spectra on π^+, π^-, K^+, K^-, p, ($\bar{p}$) at midrapidiy ($|y| < 0.5$) from Pb-Pb collisions at $\sqrt{s_{NN}} = 2.76\,\text{TeV}$ from [4].

For the 20% most central Pb-Pb collisions at midrapidiy ($|y| < 0.5$) there is additional data on K^* and ϕ from [6], on K^0_s and Λ from [7] as well as for the multistrange baryons $\Xi^\pm$ and $\Omega^\pm$ from [8]. Data on d and ^3He is obtained from [9].

The individual particles and the covered p_T ranges are shown in Table 3.1.

Particle	exp. p_T range (GeV/c)	fit range (GeV/c)
π^-	0.1–3.0	0.4–1.5
π^+	0.1–3.0	0.4–1.5
K^-	0.2–3.0	0.6–2.0
K^+	0.2–3.0	0.2–2.0
K^0_s	0.4–12.0	0.2–2.0
K^*	0.3–5.0	0.3–5.0
$\bar{p}$	0.3–4.6	0.3–3.2
p	0.3–4.6	0.3–3.2
ϕ	0.5–5.0	0.5–5.0
$\bar{\Lambda}$	0.6–12.0	0.6–3.0
Λ	0.6–12.0	0.6–3.0
Ξ^+	0.6–8.0	0.6–3.0
Ξ^-	0.6–8.0	0.6–3.0
Ω^+	1.2–7.0	1.2–3.2
Ω^-	1.2–7.0	1.2–3.2
d	0.6–4.2	0.6–4.2
^3He	2.0–8.0	2.0–5.0

Table 3.1: Transverse momentum range covered by experiment and fit range of the Pb–Pb data in the analysis of 0-20% central collisions.

Second, there are also multiplicity dependent p_T spectra on $\pi^\pm$, $K^\pm$, K^0_s, $p(\bar{p})$ and $\Lambda(\bar{\Lambda})$

Particle	exp. p_{T} range	fit range (GeV/c)
$\pi^{\pm}$	0.1–3.0	0.5–1.0
$K^{\pm}$	0.2–2.5	0.2–1.5
K^0_s	0.0–8.0	0.0–1.5
$p(\bar{p})$	0.3–4.0	0.3–3.0
$\Lambda(\bar{\Lambda})$	0.6–8.0	0.6–3.0

Table 3.2: Transverse momentum range covered by experiment and fit range of the p–Pb data in the multiplicity dependent analysis.

from p-Pb collisions at $\sqrt{s_{NN}} = 5.02\,\mathrm{TeV}$ from [10]. The available p_{T} ranges for the combined particles and antiparticles can be found in Table 3.2.

These data sets are available on HepData under [5] and [11] and are normally stored in plain ascii with the following format [12]:
xlow xhigh y +stat -stat +sys1 -sys1 +sys2 -sys2 ...
xlow and *xhigh* are the xbin edges, *y* is the measured quantity, *+stat* and *-stat* are the positive and negative statistical uncertainties (could also be +-stat if equal) and *+sysn* and *-sysn* are any number of positive and negative systematic uncertainties (again could be *+-sysn* if equal).

Since the data files correspond to specific figures or tables in the respective publication, the organization and representation of the experimental quantities is not uniform. For example there can be all centralities for one particle, stored in one table of this kind, or all particles for one centrality. In this thesis an existing C++ program [13] was used to simultaneously fit provided data for multiple particles and for each provided centrality. To convert the plain text HepData format into an ascii-file the program reads in, a C++ reader was implemented, which also converts the quantities from HepData into p_{T}-differential invariant yields if necessary. The results of the analysis have been processed and visualized with ROOT.

All of the analysis is based on statistical uncertainties only, since a systematic error resulting in a constant shift to higher or lower yields is not relevant to the parameters of the model except for the free normalization. We assume full correlations among systematic errors.

Particle	exp. p_{T} range (GeV/c)	fit range (GeV/c)
$\pi^{\pm}$	0.1–3.0	0.5–1.0
$K^{\pm}$	0.2–3.0	0.2–1.5
$p(\bar{p})$	0.3–4.6	0.3–3.0

Table 3.3: Transverse momentum range covered by experiment and fit range of the Pb–Pb publication.

The systematic errors in tracking efficiency are largely correlated, since one always needs a TPC track, independent on the TOF information available for a track or not. However, by including them we would get the same fit parameters with artificially small χ^2 values. On the other hand, there are uncorrelated systematic errors in the p_{T} range, where the particle identification in TPC and TOF overlap, which will be neglected in our approximation.

Typically, the uncertainties exhibit a similar or even smaller size than the markers of the data points in the figures. Hence, they are not visible in most cases. For example, the statistical uncertainties on the pion yields in the most central Pb-Pb collisions are 3% at most, while the systematic uncertainties are are typically one order of magnitude larger. Those relative sizes are typical for the entity of the experimental measurements evaluated in this analysis.

4 Results and Discussion

4.1 Pb–Pb multiplicity dependent spectra

In the first part of our analysis we will try to describe the multiplicity dependent p_{T} spectra for Pb–Pb at $\sqrt{s_{NN}} = 2.76\,\mathrm{TeV}$ with the Blastwave-Model. The corresponding distribution and model curves for the most central collisions and therefore highest multiplicities are shown in Figure 4.1. The fit ranges can be found in Table 3.3. Results of the Blastwave-fit are shown as colored lines and particles and antiparticles are drawn in one color with open and closed symbols. All particles in each centrality class are described by one set of parameters at the same time. The statistical uncertainties are smaller than the symbol size.

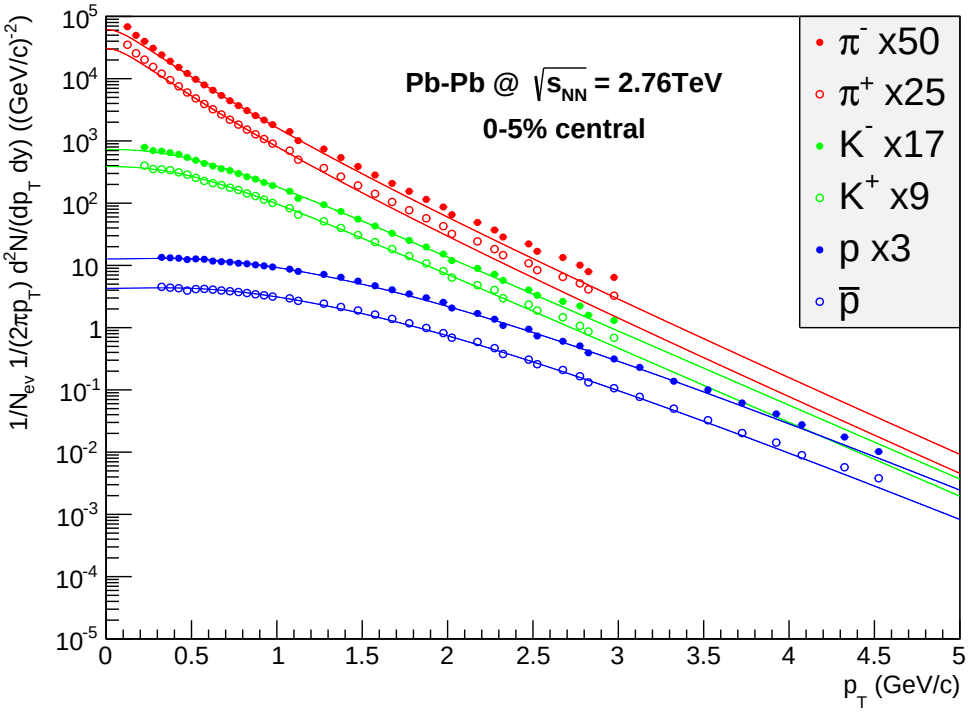

Figure 4.1: (color line) Invariant p_{T}-differential yields for $\pi^{\pm}$, $K^{\pm}$, $p(\bar{p})$ for most central Pb–Pb collisions; measured at midrapidity ($|y| < 0.5$); combined Blastwave-fit; (circles) data points; scaled for better visibility; see Table 3.3 for applied fit ranges; see Appendix for most peripheral collisions.

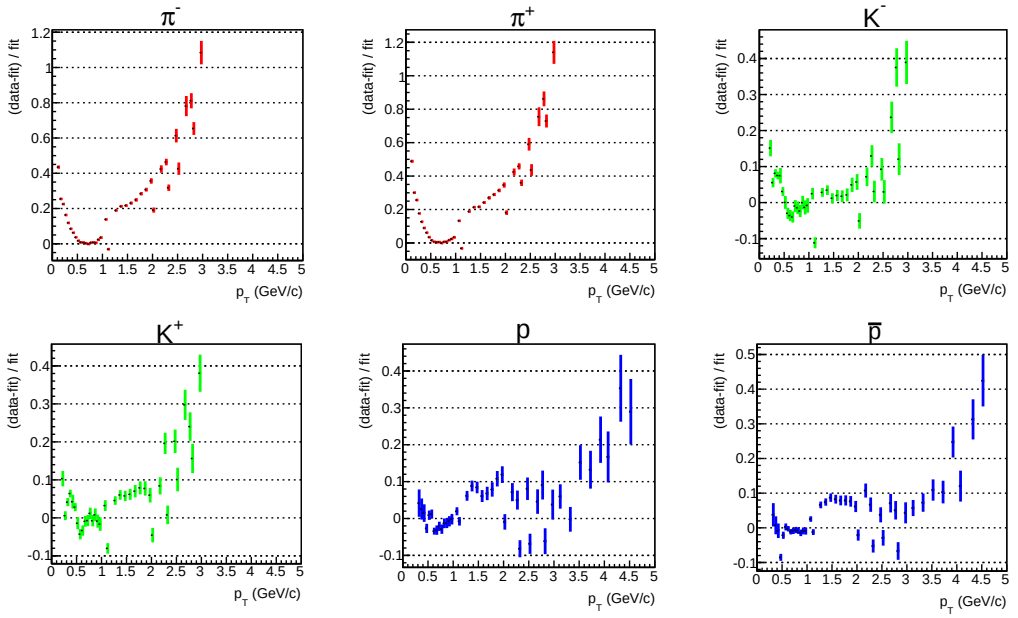

Figure 4.2: Deviation of fit and data for each particle species; shown as ratio: (data-fit)/fit; for most central Pb–Pb collisions; see Figure 4.1 for the corresponding spectrum.

The results of the combined fit for most central collisions are:
$\langle\beta_T\rangle = 0.650 \pm 0.001$, $T = (0.096 \pm 0.001)\,\mathrm{GeV}$ and $n = 0.714 \pm 0.004$

The χ^2 of the fit is 757.31 with 127 degrees of freedom. In view of the Blastwave-model's simplicity, the fit quality is rather satisfactory. The fit ranges were chosen to match the p_T interval where the Blastwave-Model is a valid description. This is easily seen in Figure 4.2, which shows the ratio of the difference between fit and data normalized to the fit. In this representation, a fit in perfect agreement with the data would show vanishing deviations, whereas a numerical value of 0.1 indicates a relative deviation by 10 %. In their respective fit ranges, all particle species agree with the model within 10 %. In the interpretation of the data we will focus on the ratio to judge the quality of the fit, since it allows to look for individual particles and the χ^2 values sometimes may be artificially enlarged by the exclusion of experimental systematic uncertainties.

At low p_T, especially for the π mesons, feed-down from particles decaying into pions e.g. $K^* \to \pi^+ + \pi^-$ or from Δ^+ populates the spectrum at $p_\mathrm{T} < 0.6\,\mathrm{GeV/c}$. This is not

Centrality class	$\langle\beta_T\rangle$	T (GeV)	n
0-5%	0.650 ± 0.001	0.096 ± 0.001	0.714 ± 0.003
5-10%	0.643 ± 0.001	0.098 ± 0.001	0.730 ± 0.004
10-20%	0.639 ± 0.001	0.099 ± 0.001	0.737 ± 0.003
20-30%	0.628 ± 0.001	0.102 ± 0.001	0.764 ± 0.004
30-40%	0.609 ± 0.001	0.105 ± 0.001	0.814 ± 0.005
40-50%	0.581 ± 0.001	0.109 ± 0.001	0.910 ± 0.007
50-60%	0.545 ± 0.001	0.114 ± 0.001	1.047 ± 0.011
60-70%	0.504 ± 0.001	0.122 ± 0.001	1.219 ± 0.018
70-80%	0.454 ± 0.002	0.130 ± 0.001	1.486 ± 0.033
80-90%	0.380 ± 0.002	0.144 ± 0.002	2.020 ± 0.086

Table 4.1: Fit-results Pb–Pb.

implemented in the Blastwave-Model. Therefore the fit range is constrained to start at 0.5 GeV/c for the pions and significant deviations can be observed at lower p_{T}.

Above p_{T} approximately 4 GeV/c for mesons and 6 GeV/c for baryons the model falls exponentially, but the spectrum is found to be much harder. This is an indication for hard perturbative QCD processes dominating the spectrum.

The model parameter dependence on centrality is depicted in Table 4.1. The mean velocity is falling and therefore particles are naively expected to be shifted towards lower p_{T}, while the freeze-out temperature is rising. In the Blastwave-Model temperature and mean velocity are not independent parameters, because a slight increase in temperature can be compensated by a slight decrease in mean velocity, while the fit quality does not change. This anti-correlation can be visualized by plotting T against $\langle\beta_T\rangle$ with their uncertainties computed as an elliptical contour showing all equally likely parameter pairs within the 68% confidence level. The centrality dependent change of the parameters can be seen in Figure 4.3, too. This can be explained by the fact, that in less central collisions the systems size and energy density are smaller, resulting in a shorter evolution time till the particles freeze-out-temperature is reached and they decouple from the system. Thus the interaction time in the medium in which collective flow can be build is reduced.

The shape parameter of the velocity profile is increasing with more peripheral collisions.

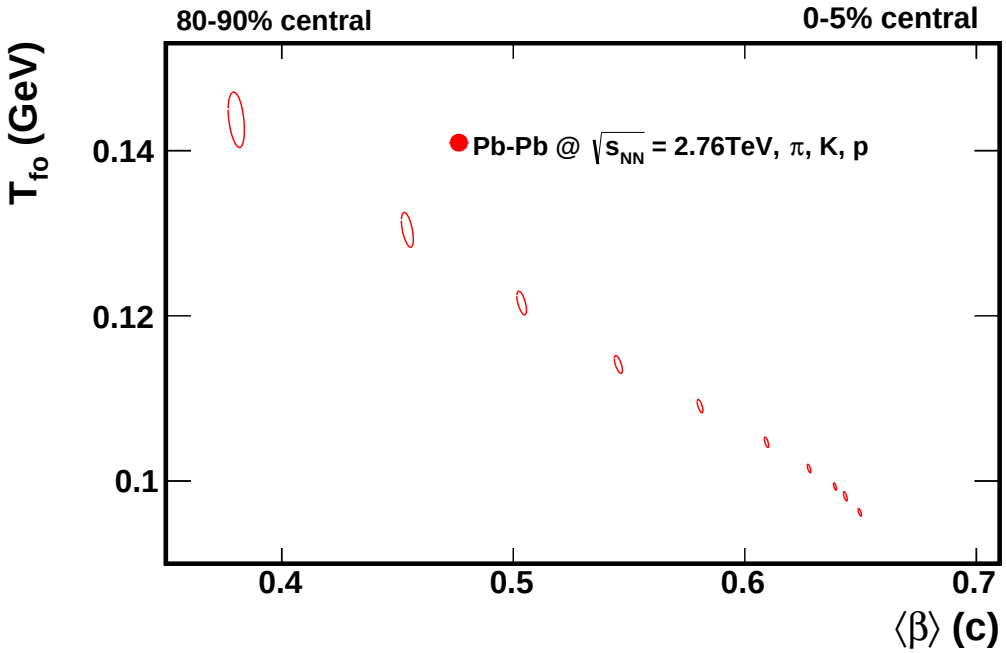

Figure 4.3: (color line) Correlations of T and $\langle\beta_T\rangle$; 1σ-contour; all centrality classes for Pb–Pb collisions at 2.76 TeV; from left to right: lowest to highest multiplicity class; see Table 4.1.

It covers a range from about 0.7 to 2.0. The velocity profile changes therefore massively from a root like to a quadratic profile with decreasing multipicity, Figure 2.2.

4.2 Pb–Pb Spectrum with all available particle species

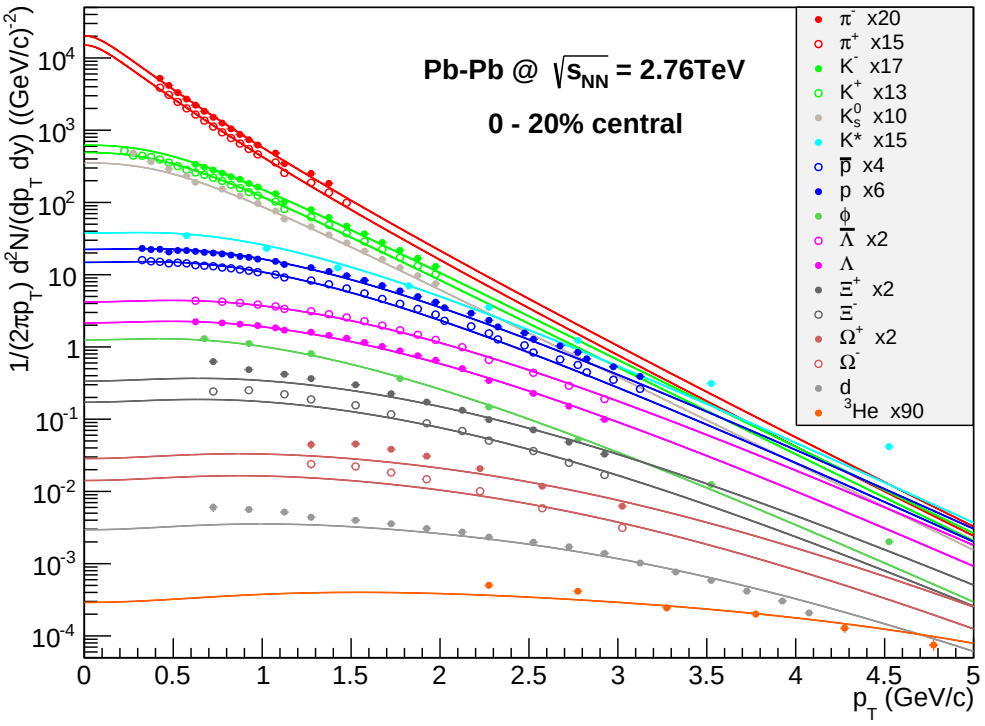

Figure 4.4: (color line) Invariant p_{T}-differential yields of 17 particle species for most central collisions measured at midrapidity; combined Blastwave-fit for all particle species; (circles) data points; scaled for better visibility; see Table 3.1 for applied fit ranges.

Since the Blastwave-Model could describe the spectra of the most abundant particles: π^+, π^-, K^+, K^- and p, $(\bar{p})$, we checked to which degree all other available hadronic particle spectra could be described within this model.

Figure 4.4 shows the invariant p_{T} spectrum for the 0-20% most central Pb–Pb collisions for 17 particle species. Particles and their charge conjugates are shown in one color with closed and open symbols, respectively, and the fit to the data is shown as colored lines. Note that a combined fit to all particles is used again, which means they are described by a single set of parameters except for the individual particle rest mass and normalization.

The fit results for the mean transverse flow velocity, the freeze-out temperature and the shape parameter of the velocity profile are only slightly changed:
$\langle\beta_T\rangle = 0.640 \pm 0.001$, $T = (0.104 \pm 0.001)\,\mathrm{GeV}$ and $n = 0.692 \pm 0.001$.

The χ^2 of the fit is 13432 with 278 degrees of freedom, which is in fact much larger than for the first analysis with only π^+, π^-, K^+, K^-, p and $(\bar{p})$. These most abundant particle species seem to constrain the results to similar values as before, due to their high statistics. The deviation of fit and data is again best visible in a plot showing their ratio, which is expected to be zero within the uncertainties for a perfect fit. In this way, we can identify p_T-regions and particles not well described by the model.

The applied fit ranges can be found in Table 3.1. In this range nearly all of the light mesons are well described by the Blastwave-Model. The K^0_s shows an enhancement at $p_\mathrm{T} < 0.5\,\mathrm{GeV/c}$, while on the high p_T side the meson and proton spectra are generally harder than the model prediction, as expected. The K^* resonance is an extreme example with a ratio of up to 2.5 at about $4.5\,\mathrm{GeV/c}$. The latter implies that it may not be describable in a combined fit at all. With the resonances short lifetime of about $4\,\mathrm{fm/c}$ it is continuously generated and destroyed throughout the whole evolution.

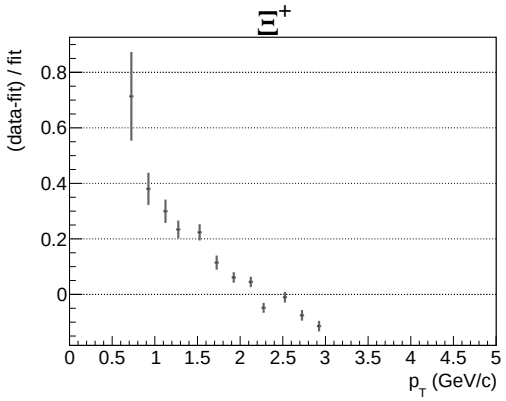

Figure 4.5: Deviation of fit and data for the positive cascade in the combined fit.

On the other hand, the baryons containing multiple strange quarks behave differently, which can be seen for example in the ratio plot of the positive cascade in Figure 4.5. Their yield is much higher than the model at low p_T (e.g. below 1.5 GeV/c for the cascades). At high p_T they tend to be lower than the fit, such that the description of the data is not satisfactory. This is also true for the deuteron and to a smaller extend

for ^3He, however low statistics and large uncertainties still allow for a reasonably good agreement here.

Since the multistrange baryons $\Xi^{\pm}$, $\Omega^{\pm}$ and the ϕ meson seem not to fit in the combined analysis, we tried to describe them on their own. The result is a much better fit with a χ^2 of 107 and 43 degrees of freedom and ratios within 10% for most data points, which can be seen in Figure 4.6. The parameters for this description are:
$\langle\beta_T\rangle = 0.572 \pm 0.039$, $T = (0.223 \pm 0.011)\,\mathrm{GeV}$ and $n = 0.223 \pm 0.308$.

The multistrange particles are found at lower collective transverse expansion velocity, but the temperature parameter is more than two times as high as in the combined analysis. The shape parameter is also lower than before suggesting a rather flat velocity profile, while the fit results easily allow for a root-like profile in the large uncertainties, too.

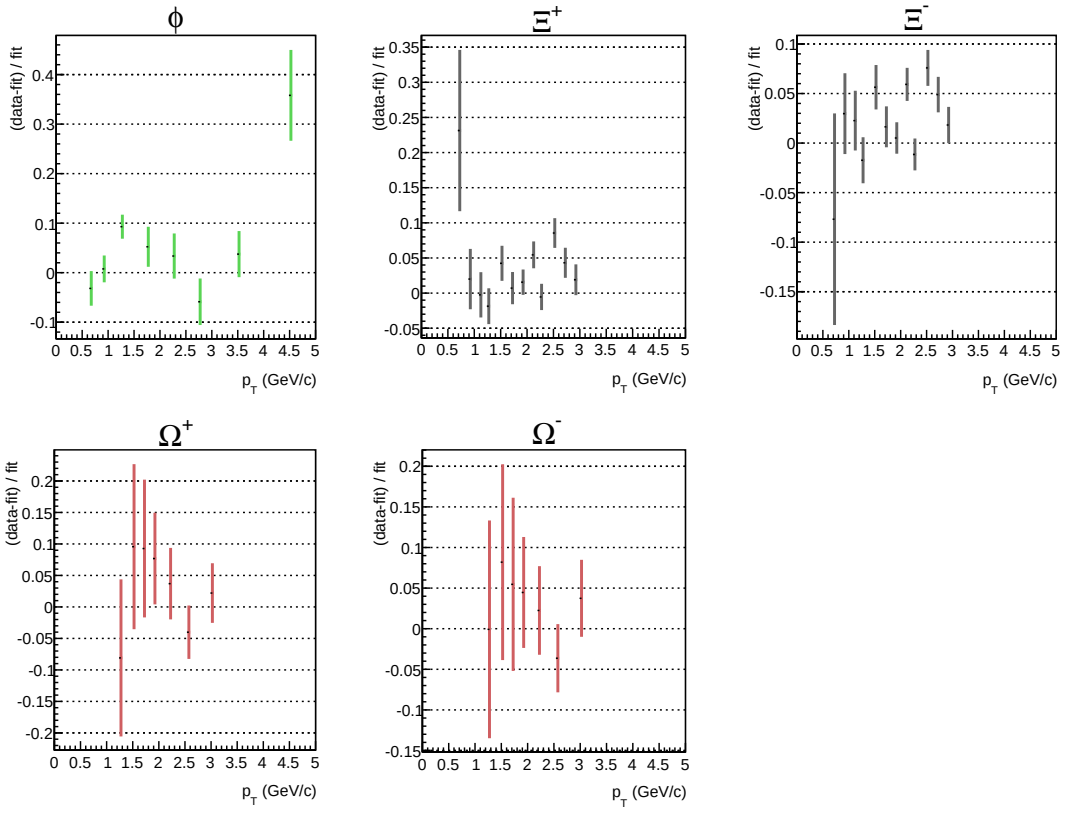

Figure 4.6: Deviation of fit and data for multistrange particles alone; shown as ratio: (data-fit)/fit; for most central Pb–Pb collisions.

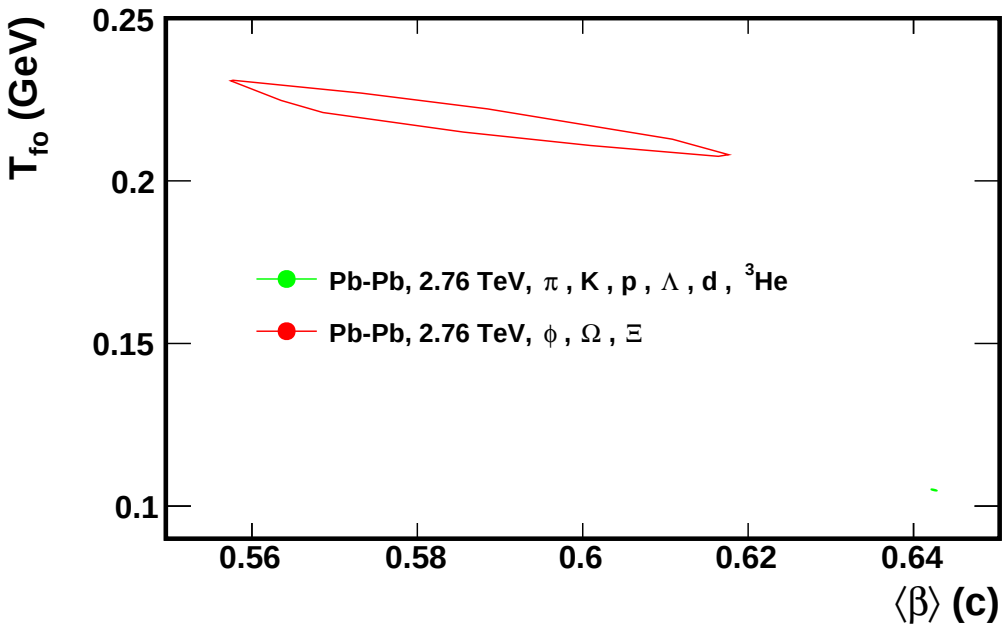

Figure 4.7: (color line) Comparison of the temperature parameter and mean transverse expansion velocity for the different particle species; 1σ-contour; 0-20% most central Pb–Pb collisions at 2.76TeV.

If we take the model parameters seriously, the substantially different set of parameters is a hint for a freeze-out of the multistrange particles not to happen at the same time as the particles containing one strange quark at most. The higher temperature suggests, that they decouple from the thermalized and collectively expanding medium before the other hadrons.

All other hadron species should be describable much better without the multistrange particles and the ϕ meson. This has been checked in an analysis of π^+, π^-, K^+, K^-, K^0_s, p, $(\bar{p})$,Λ, $\bar{\Lambda}$, d and ^3He. The K^* is left out, because the resonance was found to be not described at all before. The fit ranges were again chosen to match the published ones shown in Table 3.3, if available, or the ones used before in Table 3.1 to make the results comparable.

The ratios of this analysis show that we can describe the meson spectra within 10%, while this is only possible for the protons up to 2 GeV/c, because the experimental

points start to fluctuate from bin to bin for higher momenta. The lambda baryons are again well within 10% for all transverse momenta, whereas the deuteron and Helium yields fit within $1.7 - 4\,\mathrm{GeV/c}$ and $3 - 5\,\mathrm{GeV/c}$, respectively. The achieved agreement is satisfactory for this simple model and we can assume to describe all particle species left in this analysis with one parameter set reasonably well.

The common fit parameters are:
$\langle\beta_T\rangle = 0.642 \pm 0.001$, $T = (0.105 \pm 0.001)\,\mathrm{GeV}$ and $n = 0.669 \pm 0.001$

which is close to the previous values, due to the high statistics of pions, kaons an protons. The big difference to the multistrange particles can easily be seen in a contour plot in Figure 4.7. Even though the uncertainties of the multistrange particles are much larger than the barely visible contour at large values of $\langle\beta_T\rangle$ and lower T, the parameters are found not to be compatible with each other. These findings are consistent with results of lower energies at RHIC [14].

4.3 p–Pb multiplicity dependent spectra

After having applied the Blastwave-Model to Pb–Pb identified particle spectra, we will now look at the multiplicity dependent p_{T} spectra in p–Pb at $\sqrt{s_{NN}} = 5.02\,\mathrm{TeV}$, shown in Figure 4.8 for the highest multiplicity. All particle species in one multiplicity class are fitted simultaneously in the fit ranges shown in Table 3.2. In this data set, the yields of particles and antiparticles were found to be identical within uncertainty and have been combined.

Since there is a 2-in-1 magnet system at the LHC, the magnetic field strength is always the same for both beams. In the case of a proton and a lead beam with different charge per mass fraction, the Lorentz force keeping them in orbit can only be adjusted to fit in the geometry of the beam lines by having protons and lead ions circulate at different momenta. The need to run both beams at different momenta results in a center-of-mass system, which has a relativistic bosst of 0.465 units of rapidity in the laboratory frame parallel to the proton rapidity. Therefore, the acceptance of the detector is asymmetric in positive and negative rapidity and the rapidity range of the measurement was restricted to $0 < y_{\mathrm{cms}} < 0.5$ in the nucleon-nucleon center-of-mass system.

Multiplicity class	$\langle\beta_T\rangle$	T (GeV)	n
0-5%	0.561 ± 0.001	0.130 ± 0.001	1.028 ± 0.006
5-10%	0.546 ± 0.001	0.132 ± 0.001	1.089 ± 0.007
10-20%	0.531 ± 0.001	0.134 ± 0.001	1.165 ± 0.006
20-40%	0.504 ± 0.001	0.138 ± 0.001	1.290 ± 0.006
40-60%	0.462 ± 0.001	0.143 ± 0.001	1.521 ± 0.010
60-80%	0.397 ± 0.001	0.151 ± 0.001	1.991 ± 0.020
80-100%	0.302 ± 0.001	0.151 ± 0.001	3.161 ± 0.062

Table 4.2: Fit-results p–Pb.

For proton lead collisions, we try to describe the invariant momentum spectra with the same Blastwave-Model, which is shown in Figure 4.8. The results of the fit can be found in Table 4.2. For the highest multiplicity the parameters are:
$\langle\beta_T\rangle = 0.561 \pm 0.001$, $T = (0.130 \pm 0.001)\,\mathrm{GeV}$ and $n = 1.028 \pm 0.006$

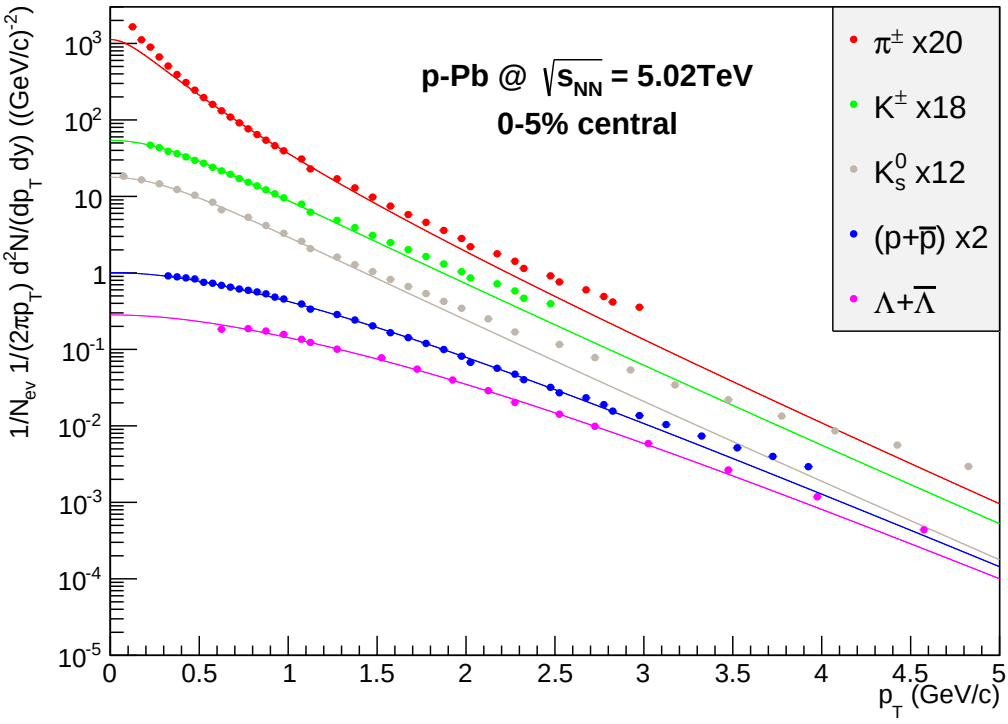

Figure 4.8: (color line) Invariant p_{T}-differential yields for $\pi^{\pm}$, $K^{\pm}$, K^0_s, $p(\bar{p})$ and $\Lambda(\bar{\Lambda})$ in the highest V0A multiplicity class; measured in the rapidity interval $0 < y_{CMS} < 0.5$; combined Blastwave-fit; (circles) data points; scaled for better visibility; see Table 3.2 for applied fit ranges; see Appendix for lowest multiplicity.

Compared to the results in the most central Pb–Pb collisions, the parameters have changed slightly. While the temperature-parameter is found to be higher than in Pb–Pb the transverse flow velocity is lower. The smalest observed shape parameter n amounts to 1.0 in p–Pb collisions. This value is larger than the corresponding one in central Pb–Pb collisions.

The quality of the description in the Blastwave-Model can again be judged by the relative deviations shown in Figure 4.9 for all measured particle species in the p–Pb publication. Relative deviations below 10% between experimental data and the Blastwave-fit are only observable in even smaller p_{T} ranges than in Pb–Pb collisions. The difference for $K^{\pm}$

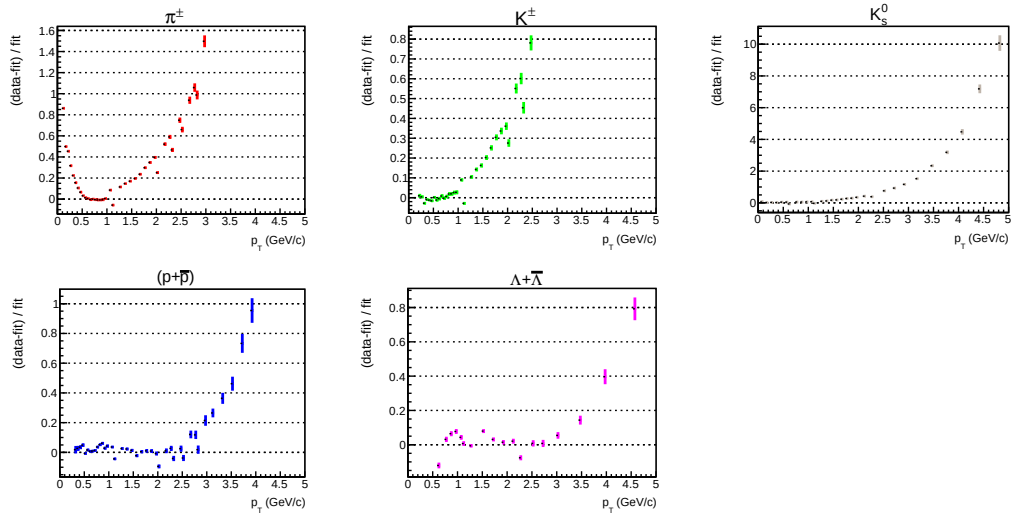

Figure 4.9: Deviation of fit and data for each particle species; shown as ratio: (data-fit)/fit; for highest multiplicity p–Pb collisions; see Figure 4.8 for the corresponding spectrum.

(protons/antiprotons) remain below 10% for $p_{\mathrm{T}} < 1\,\mathrm{GeV/c}$ ($p_{\mathrm{T}} < 2.5\,\mathrm{GeV/c}$) instead of $p_{\mathrm{T}} < 2\,\mathrm{GeV/c}$ ($p_{\mathrm{T}} < 3.5\,\mathrm{GeV/c}$) in lead-lead collisions. This and the generally slower collective expansion of the fireball with $\langle\beta_T\rangle = 0.561$, compared to $\langle\beta_T\rangle = 0.650$ in the most central Pb–Pb events, are hints of less collectivity than in lead-lead collisions. Nevertheless, the Blastwave-Model seems to be a valid description for the p_{T}-differential yields of hadrons originating from p–Pb collisions, too.

Qualitatively, the observed systematic trends for the parameters as a function of multiplicity are the same in p–Pb and in Pb–Pb collisions. The expansion velocity is constantly falling, while the temperature is constantly rising except for the very last multiplicity class (80-100%). The temperature-parameter does not rise further in that particular multiplicity class at much lower mean transverse expansion velocity. The shape parameter n reaches a value of more than 3, which indicates a rather abrupt rise of expansion velocity in the outer part of the source (see Figure 2.2). The anti-correlation of $\langle\beta_T\rangle$ and T can again be seen in Figure 4.10, showing a contour plot with the possible parameter pairs of $\langle\beta_T\rangle$ and T for all multiplicity classes available.

A summary of the obtained parameters in the analysis of Pb–Pb and p–Pb can be found in Figure 4.11. We also compare here the results to the analysis, which was performed in

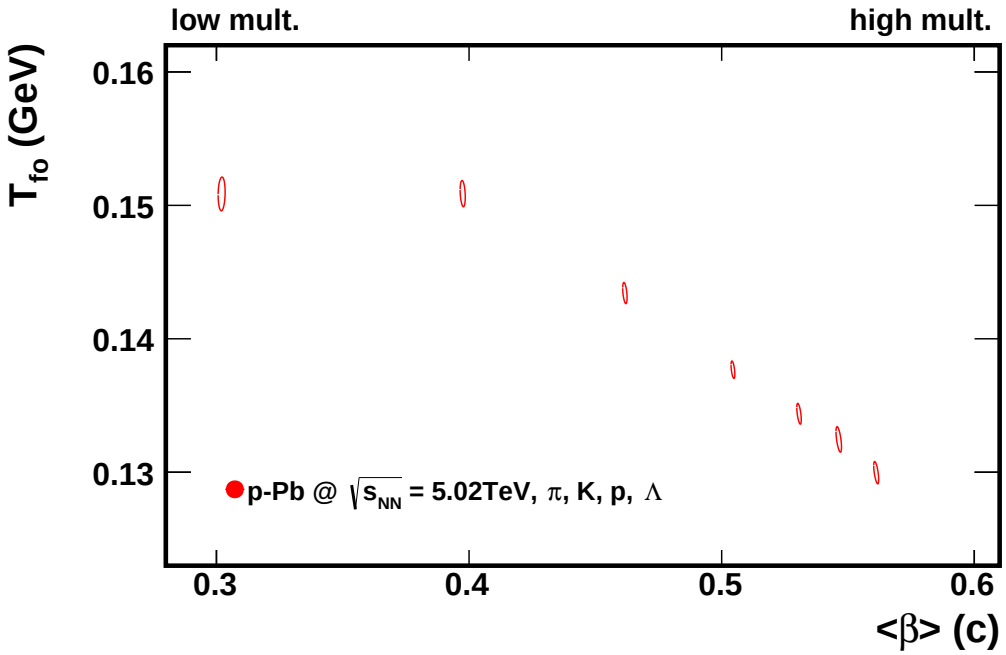

Figure 4.10: (color line) Correlations of T and $\langle\beta_T\rangle$; 1σ-contour; all multiplicity classes for p–Pb collisions at 5.02 TeV; from left to right: lowest to highest multiplicity class; see Table 4.2.

the respective original publication of the data. The results should be compatible, since the same data set, fit ranges and particle species were used.

While the parameters of Pb–Pb collisions match for central collisions and are only slightly shifted towards higher $\langle\beta_T\rangle$ and lower T for peripheral ones, the parameters for p–Pb are found to show differences. Both of our parameter sets being shifted to somewhat lower temperature and stronger collective expansion could be a hint of a systematic effect. This observation is related to the use of statistical uncertainties only, emphasizing the low-p_{T} part of the spectrum.

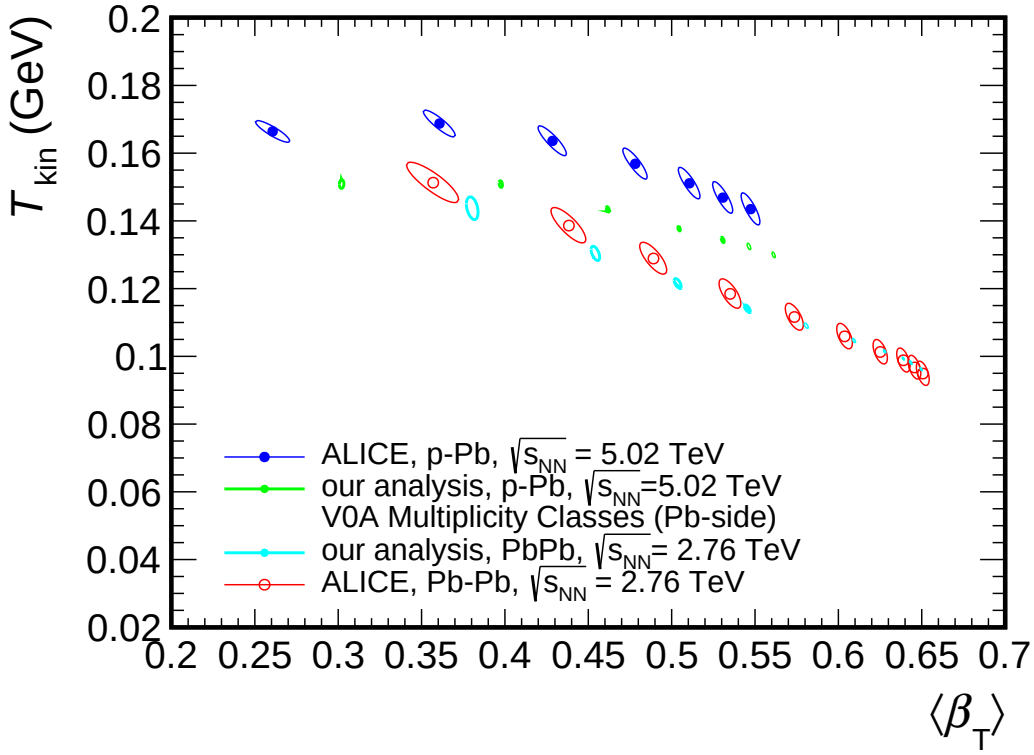

Figure 4.11: (color line) Correlations of T and $\langle\beta_T\rangle$; 1σ-contour; all centrality classes for Pb–Pb as well as p–Pb; from left to right: lowest to highest multiplicity class; compared to the results of the analysis in [10].

4.4 Predictions

Based on the results of the promising Blastwave-analysis, we want to use now the obtained information on the collective medium properties in order to predict the p_{T}-differential yields for a hypernucleus in Pb-Pb. We consider the case of the nucleus of tritium (triton), where one of the neutrons is exchanged with a Lambda baryon, called hypertriton ($_{\Lambda}{}^{3}H$). We will use the parameters that provided a good description of all particle species in most central collisions except the multistrange ones (see Section 4.2). The overall normalization is chosen to match predicted particle yields from statistical model fits [15].

The resulting spectrum is shown in Figure 4.12, where the prediction of the yield is shown in blue, while the orange curves indicate the systematic uncertainty range for higher or lower integrated yields, assumed for the normalization. In the statistical model these yields correspond to temperature-parameters of $T = 156\,\mathrm{MeV}$, $T = 164\,\mathrm{MeV}$ and $T = 152\,\mathrm{MeV}$, respectively.

Measurements of the yield of $_{\Lambda}{}^{3}H$ is work in progress by the ALICE Collaboration [16, 17].

Similar to the example above we can predict the spectral shape for D- and even heavier B-mesons. We intend to compare to calculations for pp collisions, in order to derive the nuclear modification factor R_{AA}. Therefore we use model calculations from FONLL for the cross section of the mesons in pp collisions at $\sqrt{s_{NN}} = 2.76\,\mathrm{TeV}$ and $\sqrt{s_{NN}} = 5.5\,\mathrm{TeV}$, which is the target energy for the Pb–Pb run at the LHC in 2015-2017, respectively. The calculations with the FONELL framework were provided by J. Wilkinson[18], while the details are described in [19, 20].

The nuclear modification factor is defined as

$$R_{AA} = \frac{(dN/dp_{\mathrm{T}})|_{PbPb}}{\langle T_{AA}\rangle \cdot (d\sigma/dp_{\mathrm{T}})|_{pp}}$$

with the geometrical nuclear overlap function, which is the ratio of the mean number of binary collisions and the inelastic cross section: $\langle T_{AA}\rangle = \langle N_{coll}\rangle/\sigma_{inel}^{NN}$.

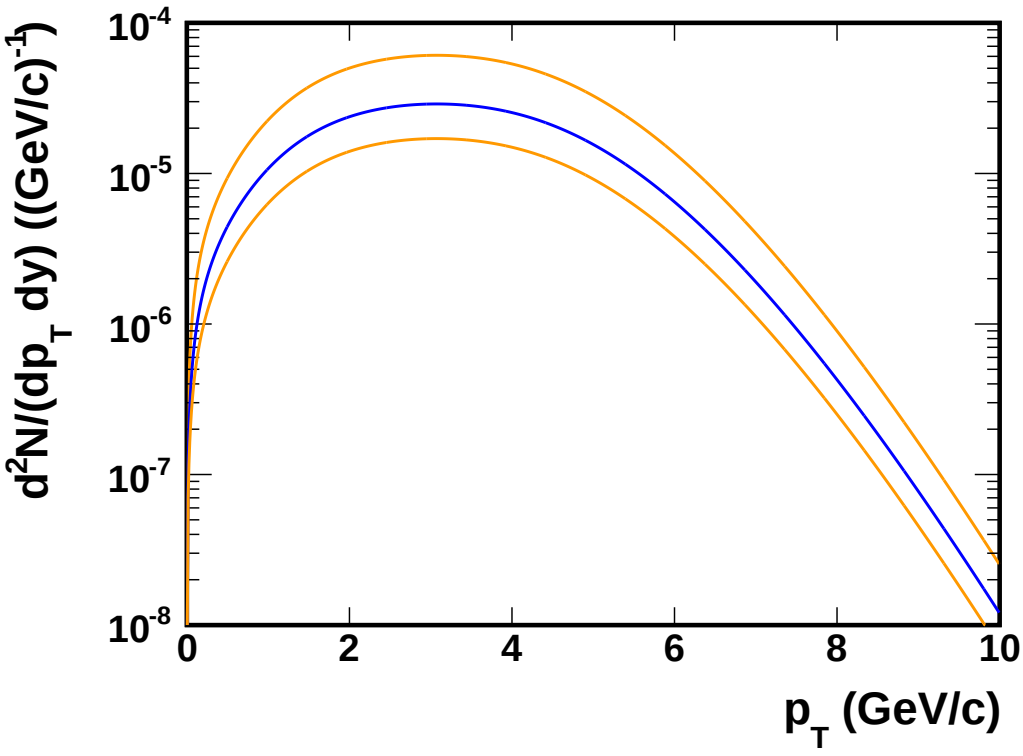

Figure 4.12: (color line) prediction for p_{T}-differential yields for hypertriton; 0-20% most central Pb-Pb collisions; best normalization shown in blue; systematic variation with normalization shown in orange.

Since we do not have information about the overall normalization in Pb–Pb collisions, we will assume, that the production of charm and bottom scales with the number of binary collisions, when going from pp to Pb–Pb, i.e.

$$\int (dN/dp_{\mathrm{T}})|_{PbPb}\ \mathrm{d}p_{\mathrm{T}} \;=\; \langle T_{AA}\rangle \int (dN/dp_{\mathrm{T}})|_{pp}\ \mathrm{d}p_{\mathrm{T}}\,.$$

At the energy of the LHC nuclear modifications are expected mainly due to shadowing. However, the effects of shadowing due to modifications of the gluon distribution in Pb are found to be smaller than 10% in theory calculations [21] and will be neglected in our approximation.

The result of the calculation can be found in Figure 4.13 for the D mesons and in Figure 4.14 for the $B^{\pm}$ mesons. Since heavy particles are not much affected by a change

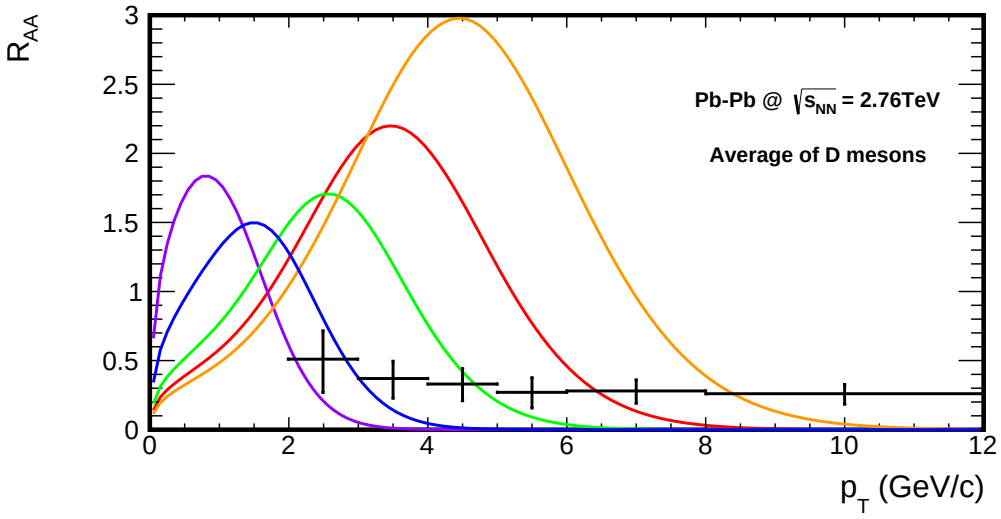

Figure 4.13: (color lines) R_{AA} prediction for D^0 mesons; different mean transverse expansion velocities: 0.40(purple), 0.50(blue), 0.60(green), 0.646(red) and 0.674(orange); based on Blastwave-Model and FONLL calculations; experimental data (black) from [22].

in temperature, we use different mean expansion velocities to estimate the systematic uncertainty. In both cases we show the result based on our analysis in red with $\langle\beta_T\rangle = 0.646$, while a range of about ± 0.04 is shown in orange and green, respectively. Both figures show also 2 curves in purple and blue as a reference for what is expected with lower collective expansion.

When assuming that Pb–Pb collisions are described by the same mechanisms as pp collisions, we would expect a flat nuclear modification factor $R_{AA} \equiv 1$, while differences indicate processes in Pb–Pb shifting particles to lower or higher p_{T}.

Looking at our best prediction (red) for the D mesons in Figure 4.13, we see a depopulation of the particle spectrum at $p_{\mathrm{T}} < 2\,\mathrm{GeV/c}$ and an enhancement of up to 200% at about $3.75\,\mathrm{GeV/c}$, compared to the pp reference. At higher p_{T} (about $6\,\mathrm{GeV/c}$) the modification factor is rapidly falling to zero, which is caused by our exponentially falling Blastwave-Model. Thus no yield is left at high p_{T}. A physical interpretation to this would be infinite energy loss for particles produced at high p_{T} in nucleus nucleus collisions, whereas the depopulation at low p_{T} is due to the collective flow in Pb–Pb,

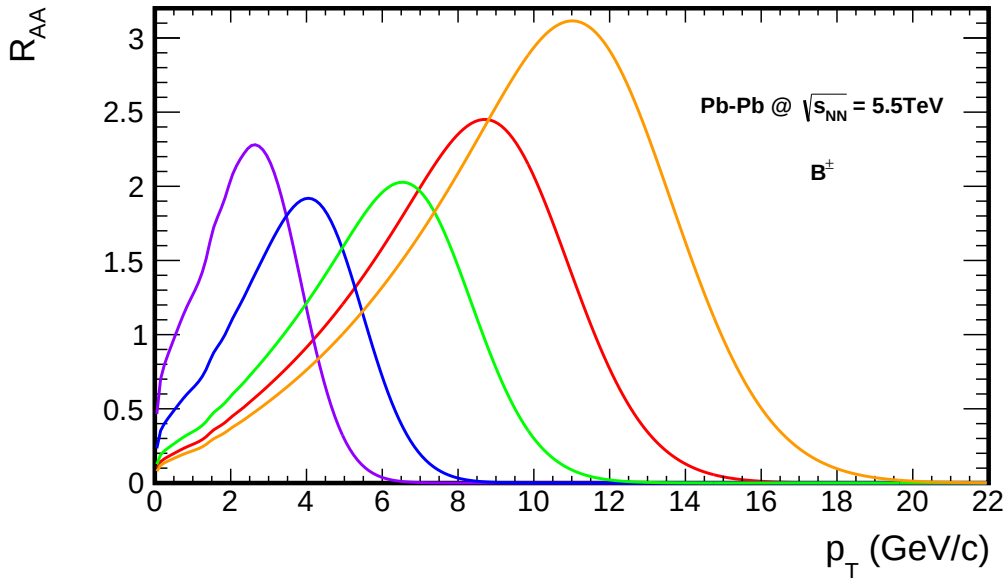

Figure 4.14: (color lines) R_{AA} prediction for $B^{\pm}$ mesons; different mean transverse expansion velocities: 0.40(purple), 0.50(blue), 0.60(green), 0.646(red) and 0.674(orange); based on Blastwave-Model and FONLL calculations.

pushing particles to larger p_{T}. The assumption of a larger mean transverse expansion velocity therefore results in a more pronounced shift to larger p_{T} (orange). When looking at collective expansions as low as $\langle\beta_T\rangle = 0.4$ (purple) the decrease is gone and the sharp increase at about 1 GeV/c is mostly due to the compensation of the rapidly falling Blastwave-Model.

The experimental data from [22] for the average R_{AA} of D^0, D^+ and D^{*+} is shown in black for the 0–20% centrality class. The data points are falling slightly for $2-5\,\mathrm{GeV/c}$ and stay nearly constant at approximatly 0.25, whereas our predictions are falling down to zero. Since the experimental data is only available at moderate to high p_{T}, the comparison to the predictions of our model is limited. However the data indicates that the parameters of the Blastwave-Model obtained in the analysis of mainly pions, kaons and protons does not describe the charmed mesons satisfactorily. The slightly falling data is much better describable by the curves in purple and blue, corresponding to $\langle\beta_T\rangle = 0.4$ and $\langle\beta_T\rangle = 0.5$, respectively. This indicates, that the charmed D mesons are found to have substantial collective flow, however not as much as the most abundant

particles.

Results from microscopic transport calculations of charm quarks in a quark gluon plasma [23] show a similar shape in R_{AA} as our prediction for $\langle\beta_T\rangle = 0.5$. In these calculations, elastic and inelastic collisions of charm quarks with constituents of the expanding medium are taken into account. The nuclear modification factor exhibits a large bump-like structure close to 2 GeV/c with a maximum value of $R_{AA} \approx 1.3$. For large momenta above 8 GeV/c, R_{AA} is flat around $R_{AA} \approx 0.15$, which is different from our model for reasons discussed above.

In Figure 4.14, the modification factor for the B mesons at $\sqrt{s_{NN}} = 5.50$ TeV shows a qualitatively similar behavior, with the high mass of the mesons making the R_{AA} extend up to 20 GeV/c and the decrease at low momenta still being visible for $\langle\beta_T\rangle = 0.40$ (purple). Measurements of this quantity are planned for 2019-2022 at LHC.

5 Conclusion

A simple Blastwave-Model was used in this thesis to describe identified particle spectra in Pb–Pb and p–Pb collisions for a variety of particle species at different multiplicities, including deuteron and ^3He nuclei in case of Pb–Pb. For p–Pb collisions, we were able to describe the spectra with the same model, finding similar but less pronounced features as in Pb–Pb. The approximate applicability of this model to p–Pb data can be interpreted as a sign of collective effects. The model parameters, that successfully described the spectra, were used to predict the p_{T}-differential yield of hypertriton in Pb–Pb.

It was shown, that multistrange particles ($\Xi^{\pm}$, $\Omega^{\pm}$, ϕ) are not described in a common fit together with most of the other particle species. A separate fit yields to larger temperature-parameters and lower collective flow velocities. This can be interpreted as an earlier decoupling from the system.

Finally, we gave predictions for the nuclear modification factor of D and $B^{\pm}$ mesons. Those calculations are based on binary scaling of the total charm and bottom cross section, the common Blastwave-fit parameters extracted from the other particle species and the theoretical prediction of the spectral shapes based on pQCD in pp collisions. The comparison to experimental data for the D mesons shows signs, that the collective flow describing the spectra is lower than expected from the analysis of light hadrons. The corresponding experimental spectra of the $B^{\pm}$ mesons will be measured at the LHC in 2019-2022.

References

[1] E. Schnedermann, J. Sollfrank and U. W. Heinz, *"Thermal phenomenology of hadrons from 200-A/GeV S+S collisions,"* Phys. Rev. C **48**, 2462 (1993) [nucl-th/9307020].

[2] S. Chatrchyan *et al.* [CMS Collaboration], *"Observation of long-range near-side angular correlations in proton-lead collisions at the LHC,"* Phys. Lett. B **718**, 795 (2013) [arXiv:1210.5482 [nucl-ex]].

[3] B. Abelev *et al.* [ALICE Collaboration], *"Long-range angular correlations on the near and away side in p-Pb collisions at* $\sqrt{s_{NN}} = 5.02\,\mathrm{TeV}$*,"* Phys. Lett. B **719**, 29 (2013) [arXiv:1212.2001].

[4] B. Abelev *et al.* [ALICE Collaboration], *"Centrality dependence of* π*, K, p production in Pb-Pb collisions at* $\sqrt{s_{NN}} = 2.76\,\mathrm{TeV}$*,"* Phys. Rev. C **88**, 044910 (2013) [arXiv:1303.0737 [hep-ex]].

[5] http://hepdata.cedar.ac.uk/view/ins1244523 .

[6] ALICE Collaboration, *"*$K^*(892)^0$ *and* $\phi(1020)$ *resonances in Pb–Pb collisions at* $\sqrt{s_{NN}} = 2.76\,\mathrm{TeV}$*,"* to be submitted.

[7] B. B. Abelev *et al.* [ALICE Collaboration], *"*K^0_S *and* Λ *production in Pb-Pb collisions at* $\sqrt{s_{NN}} = 2.76\,\mathrm{TeV}$*,"* Phys. Rev. Lett. **111**, 222301 (2013) [arXiv:1307.5530 [nucl-ex]].

[8] B. B. Abelev *et al.* [ALICE Collaboration], *"Multi-strange baryon production at mid-rapidity in Pb-Pb collisions at* $\sqrt{s_{NN}} = 2.76\,\mathrm{TeV}$*,"* arXiv:1307.5543 [nucl-ex].

[9] N. Sharma and A. Kalweit, *"Nucleus and anti-nucleus production in pp and in Pb–Pb collisions at LHC energies,"* ALICE Internal Note (CERN) https://aliceinfo.cern.ch/Notes/node/179 .

[10] B. B. Abelev *et al.* [ALICE Collaboration], *"Multiplicity Dependence of Pion, Kaon, Proton and Lambda Production in p–Pb Collisions at* $\sqrt{s_{NN}} = 5.02\,\mathrm{TeV}$*,"* arXiv:1307.6796 [nucl-ex].

[11] http://hepdata.cedar.ac.uk/view/ins1222333 .

[12] http://durpdg.dur.ac.uk/submittingdata .

[13] K. Schweda, Private communication.

[14] J. Adams *et al.* [STAR Collaboration], *"Experimental and theoretical challenges in the search for the quark gluon plasma: The STAR Collaboration's critical assessment of the evidence from RHIC collisions,"* Nucl. Phys. A **757**, 102 (2005) [nucl-ex/0501009].

[15] J. Stachel, A. Andronic, P. Braun-Munzinger and K. Redlich, *"Confronting LHC data with the statistical hadronization model"*, Proceedings of Strange Quark Matter 2013 Conference, to be published in J. Phys. G, arXiv:1311.4662 [nucl-th].

[16] R. Lea, *"Hypernuclei production in Pb–Pb collision at* $\sqrt{s_{NN}} = 2.76\,\text{TeV}$ *with ALICE at LHC,"* ALICE Internal Note (CERN) https://aliceinfo.cern.ch/Notes/node/117 .

[17] N. A. Martin, *"Investigation of light (anti-)nuclei and (anti-)hypernuclei with ALICE at the LHC (CERN),"* Master Thesis, Darmstadt, (2011) (unpublished)

[18] J. Wilkinson, Private communication.

[19] J. Wilkinson, *"Analysis and Extrapolation of D Meson Cross Sections at the LHC,"* Bachelor Thesis, (2011) http://www.physi.uni-heidelberg.de//Publications/bachelor-jeremy-wilkinson.pdf .

[20] H. Cakir, *"Precise Determination of the* $c\bar{c}$ *Cross Section in proton-proton Collisions at* $\sqrt{s} = 7\,\text{TeV}$*,"* Bachelor Thesis, Heidelberg, (2013) http://www.physi.uni-heidelberg.de//Publications/cakir_bachelor_thesis.pdf .

[21] K. J. Eskola, H. Paukkunen and C. A. Salgado, *"EPS09: A New Generation of NLO and LO Nuclear Parton Distribution Functions,"* JHEP **0904**, 065 (2009) [arXiv:0902.4154 [hep-ph]].

[22] B. Abelev *et al.* [ALICE Collaboration], *"Suppression of high transverse momentum D mesons in central Pb-Pb collisions at* $\sqrt{s_{NN}} = 2.76\,\text{TeV}$*,"* JHEP **1209**, 112 (2012) [arXiv:1203.2160 [nucl-ex]].

[23] J. Uphoff, O. Fochler, Z. Xu and C. Greiner, *"Open Heavy Flavor in Pb+Pb Collisions at* $\sqrt{s} = 2.76\,\mathrm{TeV}$ *within a Transport Model,"* Phys. Lett. B **717**, 430 (2012) [arXiv:1205.4945 [hep-ph]].

6 Appendix

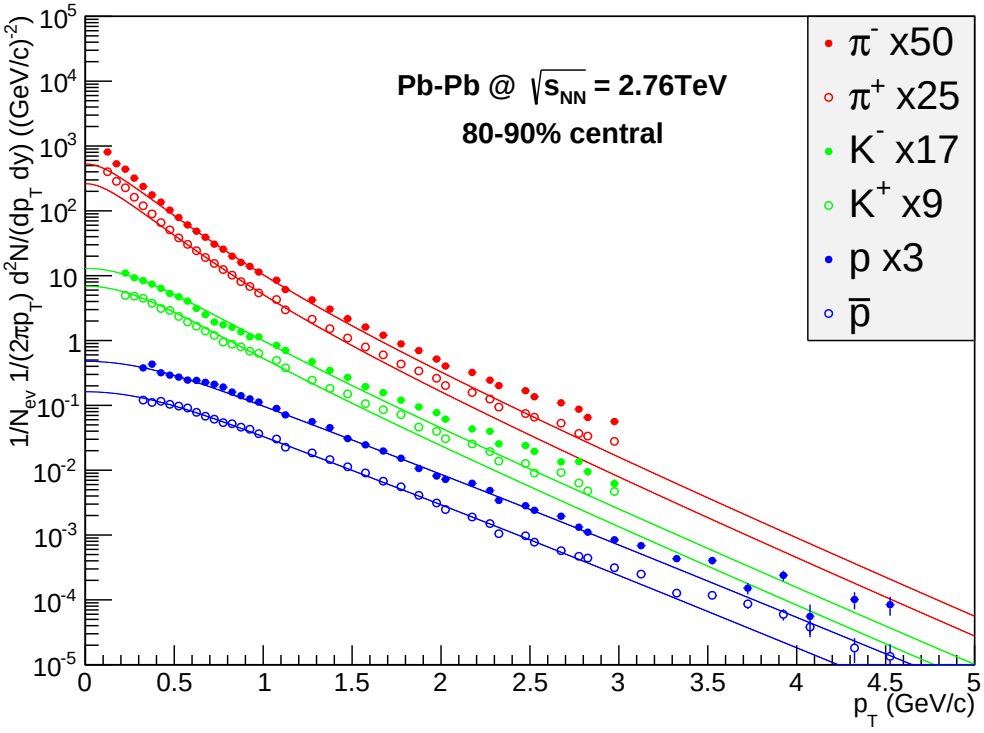

Figure 6.1: (color line) Invariant p_{T}-differential yields for $\pi^{\pm}$, $K^{\pm}$, $p(\bar{p})$ for most peripheral Pb–Pb collisions; measured at midrapidity ($|y| < 0.5$); combined Blastwave-fit; (circles) data points; scaled for better visibility; see Table 3.3 for applied fit ranges.

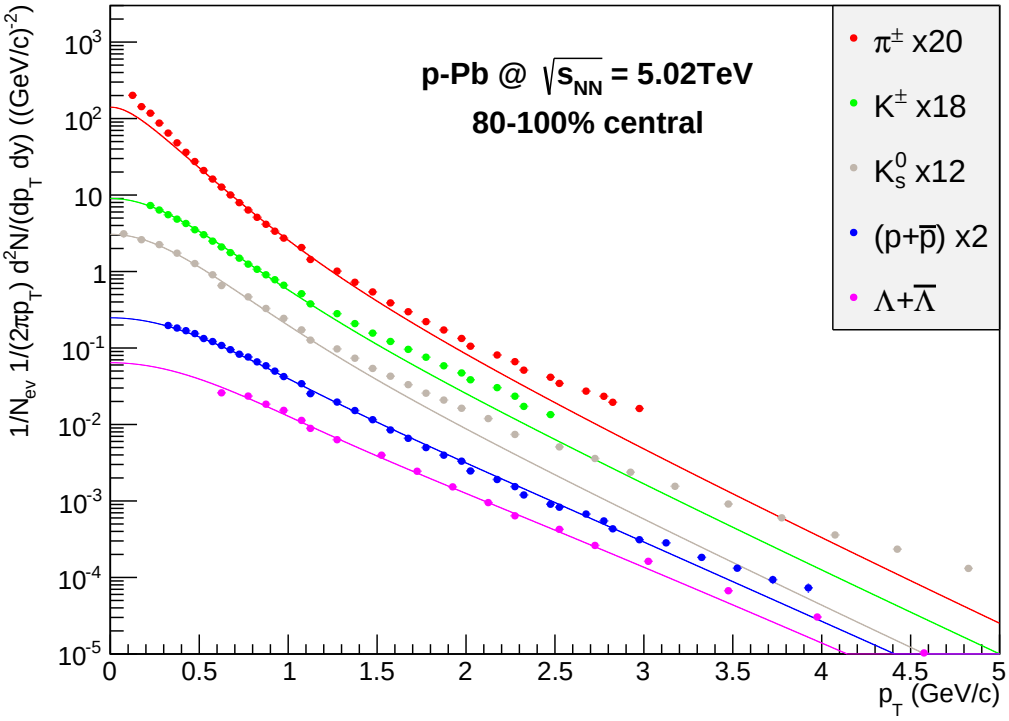

Figure 6.2: (color line) Invariant p_{T}-differential yields for $\pi^{\pm}$, $K^{\pm}$, K^0_s, $p(\bar{p})$ and $\Lambda(\bar{\Lambda})$ in the lowest V0A multiplicity class; measured in the rapidity interval $0 < y_{CMS} < 0.5$; combined Blastwave-fit; (circles) data points; scaled for better visibility; see Table 3.2 for applied fit ranges.

Acknowledgements

First of all, I would like to thank my supervisor Dr. Kai Schweda, for his help and guidance. I took great benefit from his explanations about physics and the vivid discussion on the results of my thesis. Many thanks for the motivating talks, especially when time passed too fast, too.
I want to thank Dr. Klaus Reygers for evaluating my thesis.
I also want to thank Yifei Wang for his assistance while setting up everything at the beginning and later on, especially with ROOT.
Special thanks go to Michael Winn for proofreading my thesis, giving detailed comments and for his help with theoretical problems.
Moreover, I would like to thank Dr. Benjamin Dönigus for providing the data for the analysis of the various particle species and for patiently answering my questions. I also thank Nicole Martin for her help with some related questions.
I greatly appreciate the support by Dr. Alexander Kalweit, Dr. Roberto Preghenella and Dr. Michele Floris. Thanks for providing the published contour plot for a comparison with my results and their help to understand the differences.
I also want to thank Jeremy Wilkinson for providing the FONLL calculations, the predictions of the nuclear modification factors are based on.
I wish to express my gratitude to my parents for their constant support of my studies.

This work has been supported by the Federal Ministry of Education and Research under promotional reference 06HD197D and by the Helmholtz Alliance HA216/EMMI.

Erklärung

Ich versichere, dass ich diese Arbeit selbständig verfasst und keine anderen als die angegebenen Quellen und Hilfsmittel benutzt habe.

Heidelberg, den 09.01.2014,

.....